Lattice Dynamics of Wurtzite: CdS†*

MICHEL A. NUSIMOVICI‡ AND JOSEPH L. BIRMAN
Physics Department, New York University, University Heights, New York, New York
(Received 8 July 1966; revised manuscript received 26 October 1966)

A mixed valence-Coulomb force field has been constructed and used to calculate phonon frequencies for waves propagating in three principal directions in CdS wurtzite, and in two directions of a CdS sphalerite structure. Using calculated phonon frequencies, the observed two-phonon Raman spectrum in CdS wurtzite is interpreted. Phonon symmetries and energy shifts predicted by the model have been verified by infrared and Raman experiments. The qualitative and quantitative importance of both valence and Coulomb forces in materials like CdS is demonstrated. This has implications for interpreting phonon studies in mixed crystals with wurtzite, and with sphalerite structure. The valence-Coulomb force-field model may have general applicability to other crystals, for which a shell model cannot be applied.

1. INTRODUCTION

IN this paper we present the results of a calculation of phonon frequencies in the wurtzite structure. Our particular attention was given to CdS, but the model we used may be applicable to other materials which occur in this crystal structure and which (presumably) have similar mixed binding, including mixed crystals. As will be discussed below, the model which we used included short-range forces designed to simulate the covalent-bond contributions to the potential energy; and also the long-range Coulomb force designed to represent those forces whose origin is in the partially ionic nature of the binding. We are not aware of any previous treatments of lattice dynamics in structures with mixed binding in which these particular approximations have been used to calculate the phonon dispersions. Using single-phonon energies obtained optically, we determined the seven force constants of the model, and calculated phonon dispersion in zone directions Γ-A, Γ-K, Γ-M in wurtzite and in zone directions Γ-Λ and Γ-M in a "sphalerite" form of CdS. In another paper we shall report on the calculation of one-phonon and two-phonon density of states from our model, and comparison with experiment.

In our work we found it necessary to reassign two of the single-phonon modes whose symmetry was previously incorrectly given. The revised assignments were independently confirmed by Raman scattering experiments. We also found a shift in energy of two active single-phonon wurtzite modes (Γ_1 and Γ_5) with polarization, which was apparently recently confirmed by infrared measurements. Our calculated phonon frequencies enable us to interpret the reported two-phonon Raman spectrum of CdS. Finally, our work indicates the qualitative and quantitative importance of both short-range and long-range ionic forces for the phonon spectrum in the CdS wurtzite structure. Presumably this conclusion applies as well to other wurtzite-structure compounds, including mixed crystals.

Several recent treatments of the lattice dynamics of the wurtzite structure have been given, which differ from that presented here. In the work of Jeffrey, Parry, and Mozzi,[1] and Keffer and Portis[2] the partially covalent and partially ionic binding in the wurtzite structure was considered, in an attempt to account for observed, static, structure deformations, as distortions from the ideal wurtzite structure. The central assumption was made that the deformation from the ideal wurtzite structure was caused by effective charges $\pm fe$ on each ion, which caused static strain and polarization due to the long-range Coulomb field. Thus, these authors have effectively dealt with the long-wave elastic and piezoelectric properties in wurtzite on the basis of a rigid, nondeformable-ion model. While they achieved reasonable success in that acceptable values of the parameters gave reasonable values of the distortion parameters, their work was effectively restricted to the long-wave properties of the acoustic branch. No optic-branch frequencies were determined, nor were any dispersion effects obtained for either branch. Merten[3] later discussed the lattice dynamics of wurtzite using a general force model to obtain formulas for the elastic and piezoelectric coefficients, which again, depend on the long-wave properties of the acoustic branches of the vibration spectrum. By including the long-wave ($\eta=0$) Coulomb field, Merten obtained expressions for the long-wave optic modes. Finally, Merten discussed wurtzite and sphalerite lattice modes, using a comparison between the structures which had first proven useful[4] in comparing the electronic energy bands in the two crystalline forms. Merten's calculation of phonon

† Parts of this work were presented at the American Physical Society New York Meeting, June 1965 [Bull. Am. Phys. Soc. **10**, 616 (1965)], the American Physical Society New York Meeting, January 1966 [Bull. Am. Phys. Soc. **11**, 16 (1966)], and at the Conference de la Societe Française de Physique, Grenoble, March 1966 [J. Phys. (Paris) (to be published)].

* This work supported in part by the Aerospace Research Laboratories, Office of Aerospace Research, Wright-Patterson AFB, Ohio, under Contract No. AF(33)(615)-1746 and the U. S. Army Research Office (Durham) under Grant No. DA-ARO-(D)-124-G424.

‡ Present address: Laboratoire de physique des solides, Faculté des sciences, Université de Paris, Paris, France.

[1] G. A. Jeffrey, G. S. Parry, and R. L. Mozzi, J. Chem. Phys. **25**, 1024 (1956).

[2] F. Keffer and A. M. Portis, J. Chem. Phys. **27**, 675 (1957).

[3] L. Merten, Z. Naturforsch. **15a**, 512 (1960); **15a**, 626 (1960); **17a**, 65 (1961); **13a**, 662 (1958); **13a**, 1067 (1958); **17a**, 174 (1962); **17a**, 216 (1962).

[4] J. L. Birman, Phys. Rev. **115**, 1493 (1959).

dispersion was only schematic since he did not attempt to determine accurate values of the coupling parameters in his theory to fit a particular substance; also the restrictions upon the forces, and particularly the treatment of the Coulomb field at infinite wavelength only are severe limitations of accuracy. Kaplan[5] and Sullivan[6] have examined the applicability of the "shell model"[7] to calculation of sphalerite and wurtzite normal modes. As is well known, the "shell model" has been successful in the analysis of lattice vibrations of germanium, and similar insulators, as well as ionic crystals with simple crystal structures, such as rocksalt. After careful analysis using a general shell model they showed that 50 parameters were required for the long-wavelength expressions alone. By limiting the non-Coulomb interactions to first neighbors only, the number of parameters was reduced to 28, while a further simplification (sphalerite approximation) reduced the number of parameters to 11 and then the wurtzite and sphalerite problems become essentially identical. Unfortunately, as these authors showed,[5] even the sphalerite structure could not be uniquely analyzed on the basis of the shell model. Hence, while the shell-model equations were capable of being reduced, so that the long-wave elastic, piezoelectric, and dielectric coefficients could be obtained, formally in terms of shell-model parameters no actual calculation was presented. After the present work was completed, we learned of a rigid-ion calculation of normal modes in BeO, a wurtzite structure, by Young.[8] That calculation is in apparent serious disagreement with experimentally observed modes, including the long-wave modes.[9]

It is evident, then that there is need for actual calculation of normal-mode dispersion in wurtzite structure materials. It is also evident that the shell model, which has been successful for other materials of different binding type than, e.g., CdS, and higher symmetry, e.g., cubic, is incapable of being applied to the wurtzite structure at present. With this background in mind, we consider that the results presented here represent one step in the direction of obtaining a quantitative understanding of phonon dispersion in wurtzite.

2. SYMMETRY AND GEOMETRY OF WURTZITE: C_{6v}^4-$P6_3mc$

The symmetry of the wurtzite structure has been fully examined in many places,[10,1] from a geometrical point of view. Wurtzite may be considered as four interpenetrating hexagonal Bravais lattices, or equivalently, as two interpenetrating hexagonal-close-packed lattices. In either case the primitive cell contains four atoms: two cations and two anions. We shall, throughout this paper, take the two arbitrary structure parameters: c/a and u to have their ideal values. That is

$$c/a=(8/3)^{1/2};\quad u=\tfrac{3}{8}c=|\mathbf{u}|\,, \tag{2.1}$$

where, if $\mathbf{a}_1$, $\mathbf{a}_2$, $\mathbf{a}_3$ are the base vectors of the hexagonal Bravais net, $|\mathbf{a}_1|=|\mathbf{a}_2|=\mathbf{a}$; $|\mathbf{a}_3|=c$ and $\mathbf{u}$ measures the displacement, parallel to $\mathbf{a}_3$, of the cation hexagonal-close-packed lattice with respect to the anion hexagonal-close-packed lattice. For the ideal geometry given above, the wurtzite structure is quite similar to sphalerite. Thus in both cases each cation has anions disposed at the vertices of a tetrahedron as its four nearest neighbors; and cations in very similar orientations as 12 second-nearest neighbors. The relationship between wurtzite and sphalerite structures is easily appreciated by inspecting a "stacking diagram," or $(11\bar{2}0)$ plane section through the two structures.[11] In Fig. 1 we present a diagram showing consecutive shells of neighbors about a given Cd ion in the two structures, assuming the wurtzite to be ideal. There are four basis ions in the unit wurtzite cell; each of these ions represents a

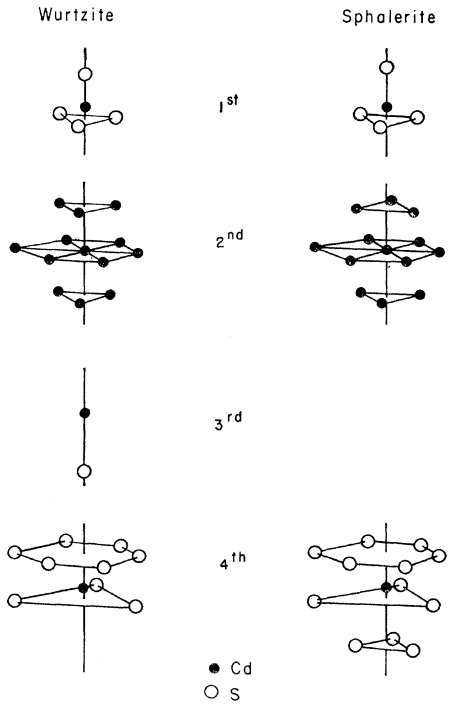

FIG. 1. Consecutive shells of neighbors of a central ion in wurtzite and sphalerite structures assuming ideal wurtzite. Shaded circles are cations, open circles are anions. Observe the similarities through the shell of second neighbors. The central ion is shown in each shell. The labeling 1st, ··· 4th refers to wurtzite. (This figure courtesy of V. A. Brophy.)

[5] H. Kaplan and J. Sullivan, Phys. Rev. **130**, 120 (1963).
[6] J. J. Sullivan, thesis, Syracuse University, 1963 (unpublished); J. Phys. Chem. Solids **25**, 1039 (1964); also D. G. Shankland, Report from Aeronautical Research Laboratories, WPAFB, Ohio, 1963 (unpublished).
[7] See, for example, B. G. Dick, in *Lattice Dynamics*, edited by R. F. Wallis (Pergamon Press, Inc., New York, 1965), p. 159.
[8] J. A. Young (private communication).
[9] R. M. Brugger, K. A. Strong, and J. M. Carpenter (to be published). We thank Dr. Brugger for sending us a report of this work prior to publication.
[10] *International Tables for X-Ray Crystallography* (Kynoch Press, Birmingham, England, 1952).
[11] Reference 4, Fig. 3.

hexagonal Bravais lattice. In Fig. 2 we show the first, second, and third neighbors of cation labeled Cd I and anion labeled S I. Each of the ions shown is involved in one or another of the springs which arise in the short-range valence forces assumed in our model, and each of the listed ions belongs to one or another of the four Bravais sublattices. The atomic coordinate positions of each atom for first and second neighbors of a given ion are already published[12] and for the single third neighbor in wurtzite are easily obtained.

The Brillouin zone of wurtzite is the well-known hexagonal prism. The Brillouin zone of sphalerite is the truncated octahedron. To facilitate comparison we give a presentation of the Jones zones of both structures,[4] on Fig. 3. The Jones zone shown here for wurtzite is simply double the usual prism; for sphalerite the Jones

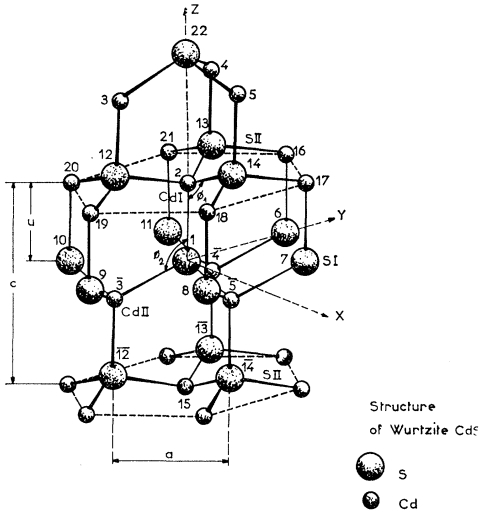

FIG. 2. First, second, and third neighbors of cation labeled Cd I and anion labeled S I. All atoms shown are involved in the short-range potential V^{SR} (see text).

and Brillouin zones are identical. Principal directions in the zone in both structures are shown on the figure.

The group theory of the wurtzite space group has been discussed by several authors[13–16] so we shall simply give a brief précis of the relevant results as needed. The space group of wurtzite is C_{6v}^4-$P6_3mc$, which we call $\mathfrak{G}$. The invariant subgroup of translations is that of the hexagonal Bravais lattice, which we call $\mathfrak{T}$. Then the factor group $\mathfrak{G}/\mathfrak{T}$ consists of 12 co-sets, whose

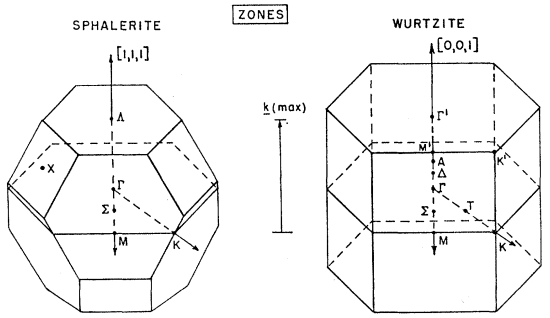

FIG. 3. The Jones zones of wurtzite and sphalerite. For sphalerite the Jones and first Brillouin zones are identical; for wurtzite the Jones zone is a double prism, i.e., double Brillouin zone.

representatives may be taken as

$$\{\varepsilon|0\},\ \{\delta_3|0\},\ \{\delta_3|0\}^{-1},\ \{\sigma_d^{(1)}|0\},\ \{\sigma_d^{(2)}|0\},\ \{\sigma_d^{(3)}|0\}, \quad (2.2)$$

and

$$\{\delta_2|\tau\},\ \{\delta_6|\tau\},\ \{\delta_6|\tau\}^{-1},\ \{\sigma_v^{(1)}|\tau\},\ \{\sigma_v^{(2)}|\tau\},\ \{\sigma_v^{(3)}|\tau\}, \quad (2.3)$$

where $\tau=\mathbf{a}_3/2$. The coset representatives (2.2) alone form a group, isomorphic to C_{3v}. The representatives (2.2) plus (2.3) do not form a group as they are not closed under multiplication. In what follows we shall at times be concerned with various subgroups of $\mathfrak{G}$, especially the subgroups which are themselves space groups: these generally consist of certain of the coset representatives (2.2), (2.3) combined with the translation group $\mathfrak{T}$. These subgroups are the groups of the wave vector $\boldsymbol{\eta}$, to be referred to later; these are generally denoted in the text as $\mathfrak{G}(\boldsymbol{\eta})$, i.e., $\mathfrak{G}(\Gamma)$, $\mathfrak{G}(A)$, etc., where the particular wave vectors $\boldsymbol{\eta}$ are defined on Fig. 3.

3. THE NORMAL-MODE PROBLEM

To determine the normal modes of motion and the corresponding phonon frequencies, we must solve the equations of motion for the ion displacements.[17] If we call the instantaneous ion position of the κth basis particle in the lth cell

$$\mathbf{r}(l,\kappa)=\mathbf{r}^0(l,\kappa)+\mathbf{u}(l,\kappa), \quad (3.1)$$

where $\mathbf{r}^0(l,\kappa)$ is the rest position of the particle, and $\mathbf{u}(l,\kappa)$ the displacement from rest, then the Cartesian components $u_\alpha(l,\kappa)$, $\alpha=1, 2, 3$ are the basic dynamical variables. In the harmonic approximation the potential energy of the lattice is

$$V=\tfrac{1}{2}\sum_{\substack{l\kappa\alpha\\ l'\kappa'\beta}} u_\alpha(l,\kappa)\Phi_{\alpha\beta}(ll',\kappa\kappa')u_\beta(l',\kappa'). \quad (3.2)$$

[12] L. Merten, Z. Naturforsch. **15a**, 512 (1960), Table 2; J. L. Birman, Ref. 4, Tables 1 and 2.

[13] G. Dresselhaus, Phys. Rev. **105**, 135 (1957); M. L. Glasser, J. Phys. Chem. Solids **10**, 229 (1959). Both of these papers give some erroneous results (see Refs. 14, 15).

[14] J. L. Birman, Phys. Rev. **114**, 1490 (1959); R. C. Casella, *ibid.* **114**, 1514 (1959); and Ref. 4.

[15] E. I. Rashba, Fiz. Tverd. Tela. **1**, 407 (1959) [English transl.: Soviet Phys.—Solid State **1**, 368 (1959)].

[16] M. Nusimovici, J. Phys. (Paris) **26**, 689 (1965). See *note added in proof* (p. 696).

[17] M. Born and K. Huang, *Dynamical Theory of Crystal Lattices* (Oxford University Press, New York, 1954), Secs. 15, 24, 38.

The equations of motion of the masses M_κ are

$$M_\kappa \ddot{u}_\alpha(l',\kappa)+\sum_{l'\kappa'\beta}\Phi_{\alpha\beta}(ll',\kappa\kappa')u_\beta(l',\kappa')=0, \quad (3.3)$$

where the dot means a time differentiation. We introduce the dynamical matrix by Fourier transformation

$$D_{\alpha\beta}(\boldsymbol{\eta},\kappa\kappa')=\sum_{\lambda}\Phi_{\alpha\beta}(\lambda,\kappa\kappa')\frac{\exp(-2\pi i\boldsymbol{\eta}\cdot\mathbf{R}_\lambda)}{(M_\kappa M_{\kappa'})^{1/2}}, \quad (3.4)$$

taking advantage of the fact that the elementary force constants $\Phi_{\alpha\beta}(ll',\kappa\kappa')$ depend only on differences $l-l'$. If we now assume that the displacement $\mathbf{u}(l,\kappa)$ has harmonic time variation, with frequency ω, the equations of motion (3.3) become

$$\sum_{\kappa'\beta} D_{\alpha\beta}(\boldsymbol{\eta},\kappa\kappa')e_\beta(\kappa'|\boldsymbol{\eta},j)=\omega^2(\boldsymbol{\eta}|j)e_\alpha(\kappa|\boldsymbol{\eta},j). \quad (3.5)$$

In (3.5) $\omega^2(\boldsymbol{\eta}|j)$ is the squared eigenfrequency for wave vector $\boldsymbol{\eta}$, branch j, and $e_\alpha(\kappa|\boldsymbol{\eta},j)$ is the αth Cartesian component of the eigenvector $\mathbf{e}(\kappa|\boldsymbol{\eta},j)$. For fixed $\boldsymbol{\eta}$, the equations (3.5) determine $3s$ eigenfrequencies (not all necessarily distinct), where s is the number of basis atoms in the cell and $3s$ the number of Cartesian mechanical degrees of freedom per cell. The eigenvalue problem (3.5) can be formulated as the determination of the eigenfrequencies $\omega^2(\boldsymbol{\eta}|j)$ of the dynamical matrix by solution of a secular determinant

$$\|\mathbf{D}(\boldsymbol{\eta})-\omega^2(\boldsymbol{\eta}|j)\mathbf{I}\|=0, \quad (3.6)$$

where $\mathbf{D}(\boldsymbol{\eta})$ is the $3s\times 3s$ dynamical matrix whose rows and columns are labeled by the indices $\alpha\beta$ and $\kappa\kappa'$, and $\mathbf{I}$ is the diagonal unit $(3s\times 3s)$ matrix. For fixed $\boldsymbol{\eta}$ and j, we can consider the $3s$ components of $e_\alpha(\kappa|\boldsymbol{\eta},j)$, $\alpha=1, 2, 3$, $\kappa=1\cdots s$ as the $3s$ rows of a column vector. Physically $e_\alpha(\kappa|\boldsymbol{\eta},j)$ gives the amplitude of the αth Cartesian component of displacement of atom κ in the normal mode of wave vector $\boldsymbol{\eta}$, corresponding to branch j, eigenfrequency $\omega(\boldsymbol{\eta}|j)$.

To determine the $\omega^2(\boldsymbol{\eta}|j)$ and the eigenvectors $e_\alpha(\kappa|\boldsymbol{\eta},j)$ we first obtain a complete set of force constants

$$\Phi_{\alpha\beta}(ll',\kappa\kappa')\equiv\left[\frac{\partial^2 V}{\partial u_\alpha(l,\kappa)\partial u_\beta(l',\kappa')}\right]_0, \quad (3.7)$$

then transform as in (3.4) to obtain $\mathbf{D}$. We treat short-range (SR) and Coulomb (C) contributions to (3.2) separately. We write for the potential energy

$$V=V^{\mathrm{SR}}+V^{\mathrm{C}}. \quad (3.8)$$

Short-Range Contribution

Under the rubric of short-range contributions to the potential energy V^{SR} we include all the near-neighbor non-Coulomb contributions. We represent V^{SR} in terms of a function which depends upon eight force constants. These represent stiffnesses opposing certain bond-length changes and changes in certain vertex angles, and are left to be determined. They represent both two-body and three-body interactions. This part of the potential energy is quite similar to the valence force models used by Herman[18] and Pope[19] in treating germanium and silicon lattice dynamics. In spite of the great vogue for "shell-model" calculations, based in part on their success in accounting for phonon spectra of germanium and silicon[20] it needs to be remarked that the calculation of Herman gave excellent agreement with experiment using fewer disposable valence-field parameters than those needed by the recent shell-model calculations in the same substances (Dolling and Cowley[7]). Also the recent work of Musgrave and Pople[21] and Musgrave[22] on phonon dispersion in diamond indicates that a valence force field model, with relatively few model parameters, and with model parameters interpretable in reasonable physical terms, can give a good quantitative account of the experimental phonon spectrum. Note, too, that valence force models with few disposable parameters go back at least to the earliest days of quantitative lattice dynamics.[23]

With these preliminaries disposed of, we write for the short-range part of the potential energy:

$$\begin{aligned}V^{\mathrm{SR}}=&\tfrac{1}{2}\sum_{1^\circ}\lambda(\delta r_{ij})^2+\tfrac{1}{2}\sum_{2^\circ\mathrm{Cd}}\mu(\delta r_{jl})^2+\tfrac{1}{2}\sum_{2^\circ\mathrm{S}}\nu(\delta r_{ik})^2\\&+\tfrac{1}{2}\sum_{3^\circ}\delta(\delta r_{il})^2+\tfrac{1}{2}\sum_{\mathrm{S\text{-}Cd\text{-}S}}k_\theta r_0^2(\delta\theta_{ij\kappa})^2\\&+\tfrac{1}{2}\sum_{\mathrm{Cd\text{-}S\text{-}Cd}}k_{\theta'}r_0^2(\delta\theta_{jkl})^2+\tfrac{1}{2}\sum_{\mathrm{Cd\text{-}S\text{-}Cd}}k_{r\theta}'r_0^2(\delta\theta_{jkl})(\delta r_{jk})\\&+\tfrac{1}{2}\sum_{\mathrm{S\text{-}Cd\text{-}S}}k_{r\theta}r_0^2(\delta\theta_{jkl})(\delta r_{jk}). \quad (3.9)\end{aligned}$$

The spring constants in (3.9) are λ, μ, ν, δ, k_θ, $k_{\theta'}$, $k_{r\theta}$, $k_{r\theta}'$. The springs λ, μ, ν, δ are two-body interactions which oppose bond extensions: in turn these represent springs opposing first-neighbor Cd-S bond extension (λ); opposing second-neighbor Cd-Cd bond extension (μ); opposing second-neighbor S-S bond extension (ν); opposing third-neighbor Cd-S bond extension (δ). (In regard to the latter see Fig. 1 for the single third neighbor in wurtzite.) The springs k_θ and $k_{\theta'}$ represent three-body interactions opposing changes in bond angles: k_θ refers to changes in first-neighbor angles S-Cd-S, while $k_{\theta'}$ to refers to changes in first-neighbor angles Cd-S-Cd. The constants $k_{r\theta}$ and $k_{r\theta}'$ are cross coupling constants, for the bond, and the angle of which the bond forms one arm. The potential-energy function

[18] F. Herman, J. Phys. Chem. Solids 8, 405 (1959).
[19] N. K. Pope, in *Lattice Dynamics*, edited by R. F. Wallis (Pergamon Press, Inc., New York, 1965), p. 147.
[20] W. Cochran, Proc. Roy. Soc. (London) **A253**, 260 (1959).
[21] M. J. P. Musgrave and J. A. Pople, Proc. Roy. Soc. (London) **268**, 474 (1962).
[22] M. J. P. Musgrave (private communication).
[23] M. Born, Ann. Phys. (Paris) 4, 44 (1914).

V^{SR} includes interactions of a given ion with its neighbors in wurtzite up to and including third neighbors, as indicated also under the summation indices in (3.9).

To utilize (3.9) in the analysis, we must evaluate the derivatives (3.7), or what is the same thing, transform from the set of independent valence force field variables to the usual Cartesian displacement variables $u_\alpha(l,\kappa)$. We require the short-range force constants

$$\Phi_{\alpha\beta}{}^{SR}(ll',\kappa\kappa')=\left[\frac{\partial^2 V^{SR}}{\partial u_\alpha(l,\kappa)\partial u_\beta(l',\kappa')}\right]_0. \quad (3.10)$$

In the evaluation and transformation it is useful to utilize the rules[21,24]

$$\left[\frac{\partial(\delta r_{ij})}{\partial u_\alpha(i)}\right]=\frac{(u_\alpha(i)-u_\alpha(j))}{r_0{}^2}, \quad (3.11)$$

$$\left[\frac{\partial\theta_{ijk}}{\partial u_\alpha(i)}\right]=\frac{1}{2\sqrt{2}r_0{}^2}[3(u_\alpha(k)-u_\alpha(j)) +(u_\alpha(i)-u_\alpha(j))], \quad (3.12)$$

and

$$\left[\frac{\partial\theta_{ijk}}{\partial u_\beta(j)}\right]=\frac{2}{\sqrt{2}r_0{}^2}[u_\beta(i)+u_\beta(k)-2u_\beta(j)]. \quad (3.13)$$

In (3.11)–(3.13) the atom index pair (l,κ) was replaced by a single index i or j, r_0 is the initial distance between the first neighbors, while r_0' is the appropriate distance between ion pairs involved in δr_{ij}. Using (3.11)–(3.13) we easily obtain the elementary short-range force matrices $\Phi_{\alpha\beta}{}^{SR}(ll',\kappa\kappa')$ from (3.7) and the corresponding $D_{\alpha\beta}{}^{SR}(\boldsymbol{\eta},\kappa\kappa')$ from (3.4). In constructing the latter we assume that the force matrix connecting atom pairs (l,κ) and (l',κ') which are farther apart than third neighbors, vanishes identically. Here we shall not enumerate the matrices $\Phi_{\alpha\beta}{}^{SR}(ll',\kappa\kappa')$ as their computation is elementary, and examples have been given by Merten.[25] Note also that use is made, in our work, of the ideal tetrahedral arrangement of the first neighbors about each ion, so that (3.12) and (3.13) must be modified for nonideal wurtzite structures.

Coulomb Contribution

To determine the Coulomb part of the force matrix we take Cd and S ions to be point ions of (unknown) charge $\pm q_\kappa$, respectively. When the ions are at instantaneous positions $\mathbf{r}(l,\kappa)$, see (3.1), the Coulomb contribution to the potential energy[17] in wurtzite is

$$V^C=\sum_{\substack{l\kappa\\ l'\kappa'}}{}' \frac{q_\kappa q_{\kappa'}}{|\mathbf{r}(l,\kappa)-\mathbf{r}(l',\kappa')|}. \quad (3.14)$$

In (3.14) the prime signifies that the divergent term due to the Coulomb self-interaction of a point charge must be omitted. The force-constant matrix element corresponding to (3.14) is typically

$$\Phi_{\alpha\beta}{}^C(ll',\kappa\kappa')=\left[\frac{\partial^2 V^C}{\partial u_\alpha(l,\kappa)\partial u_\beta(l',\kappa')}\right]_0. \quad (3.15)$$

The corresponding Coulomb contribution to the dynamical matrix is

$$D_{\alpha\beta}{}^C(\boldsymbol{\eta},\kappa\kappa')=\sum_\lambda \Phi_{\alpha\beta}{}^C(\lambda,\kappa\kappa')\frac{\exp(-2\pi i\boldsymbol{\eta}\cdot\mathbf{R}_\lambda)}{(M_\kappa M_{\kappa'})^{1/2}}$$

$$=\frac{q_\kappa q_{\kappa'}}{(M_\kappa M_{\kappa'})^{1/2}}\sum_{\lambda\equiv l-l'}{}' \exp(-2\pi i\boldsymbol{\eta}\cdot\mathbf{R}_\lambda)$$

$$\times\left[\frac{\partial^2}{\partial u_\alpha(l,\kappa)\partial u_\beta(l',\kappa')}\left(\frac{1}{|\mathbf{r}(l,\kappa)-\mathbf{r}(l',\kappa')|}\right)\right]. \quad (3.16)$$

The element $D_{\alpha\beta}{}^C(\boldsymbol{\eta},\kappa\kappa')$ may be interpreted as the αth component of the electric field at site $\mathbf{r}_{\kappa\kappa'}\equiv\mathbf{r}_\kappa-\mathbf{r}_{\kappa'}$ when a fictitious dipole wave of polarization β, wave vector $\boldsymbol{\eta}$, magnitude $q_\kappa q_{\kappa'}/(M_\kappa M_{\kappa'})^{1/2}$ exists at each lattice site of the hexagonal Bravais lattice. That is, the equivalent electric field may be defined as the dot product of a certain dyadic with a vector representing the magnitude and polarization of fictitious dipole. Writing

$$\mathbf{p}=\rho\hat{p}, \quad (3.17)$$

where $\rho=q_\kappa q_{\kappa'}/(M_\kappa M_{\kappa'})^{1/2}=-q^2/(M_\kappa M_{\kappa'})^{1/2}$, and $\hat{p}$ is a unit polarization vector, we can write

$$D_{\alpha\beta}{}^C(\boldsymbol{\eta},\kappa\kappa')=(\mathbf{B}(\boldsymbol{\eta},\kappa\kappa')\cdot\hat{p}_\beta)_\alpha, \quad (3.18)$$

where the basic object to be computed is

$$\mathbf{B}(\boldsymbol{\eta},\kappa\kappa')=\sum_\lambda{}' \exp(-2\pi i\boldsymbol{\eta}\cdot\mathbf{R}_\lambda)\left[\nabla\nabla\frac{1}{|\mathbf{r}-\mathbf{R}_\lambda|}\right]_0. \quad (3.19)$$

The gradient in Eq. (3.19) is to be taken with respect to $\mathbf{r}$; the sum there is over a hexagonal lattice.

The evaluation of (3.19) has been discussed in several places.[3,6,17,26] The most exact and general procedure utilizes the Ewald transformation, and this procedure was utilized for all results which will be presented here. Once the parameter ρ is determined, and the quantities in (3.19) computed, the contribution of the Coulomb field to the dynamical matrix element is completely determined. We discuss below how the "Coulomb" parameter was determined. The actual calculation of the quantities (3.19) was programmed as a subroutine for the New York University CDC 6600 computer. We did not obtain a printout of the values of (3.19) for each case computed, but satisfied ourselves by choosing different values of the Ewald parameter

[24] E. B. Wilson, J. C. Decius, and P. C. Cross, *Molecular Vibrations* (McGraw-Hill Book Company, Inc., New York, 1955).
[25] L. Merton, Z. Naturforsch. **17a**, 65 (1962).
[26] E. W. Kellerman, Phil. Trans. Roy. Soc. (London) **A238**, 513 (1940).

("trennungs-parameter") that the subroutine was correct for a number of test cases.

The Dynamical Matrix

Owing to the four-atom basis (CdI, CdII, SI, SII in Fig. 1) of wurtzite, there are 12 dynamical degrees of freedom per cell. Hence (3.6) is a 12×12 matrix. In sphalerite with a two-atom basis, the secular problem (3.6) is (6×6). To compose the complete dynamical matrix from its constituents we write

$$D_{\alpha\beta}(\boldsymbol{\eta},\kappa\kappa')=D_{\alpha\beta}{}^{\mathrm{SR}}(\boldsymbol{\eta},\kappa\kappa')+D_{\alpha\beta}{}^{\mathrm{C}}(\boldsymbol{\eta},\kappa\kappa'),\quad \alpha,\beta=1,2,3,\quad \kappa,\kappa'=1,2,3,4, \tag{3.20}$$

for wurtzite. For sphalerite $\kappa,\kappa'=1,2$ only.

Now to proceed with the actual calculation, we require the numerical values of the nine parameters: eight short-range, plus one Coulomb parameter. We determined the values of these parameters by fitting the expressions for the $\boldsymbol{\eta}=0$ solutions of the equation of motion (3.5) to the experimentally observed one-phonon eigenfrequencies in CdS wurtzite. At $\boldsymbol{\eta}=0$ (Γ in the Brillouin zone) the normal modes of vibration span the following irreducible representations of the point group C_{6v}-$6mm$, which is $\mathfrak{G}(\Gamma)/\mathfrak{T}$, in this case[15]:

$$2\Gamma_1\oplus2\Gamma_5\oplus2\Gamma_6\oplus2\Gamma_4, \tag{3.21}$$

as is easily seen using the standard method of placing displacement vectors upon each ion in the basis, and reducing this "displacement" representation.[16,21] One set of the representations $\Gamma_1\oplus\Gamma_5$ correspond to the acoustic branches for which $\omega^2=0$. Now using the notation $\omega^2(\boldsymbol{\eta}\,|\,j)$ we denote the squared frequency at wave vector $\boldsymbol{\eta}$, branch j. The branch index will be taken as the irreducible representation spanned by the relevent eigenvector. Thus for the three acoustic branches we have

$$\omega^2(0\,|\,\Gamma_1)=\omega^2(0\,|\,\Gamma_5)=0. \tag{3.22}$$

In taking the limit $\boldsymbol{\eta}\to0$ we found two cases to be distinguished: $\boldsymbol{\eta}\|z$, $\boldsymbol{\eta}\|x$.

For $\boldsymbol{\eta}\|z$ the secular determinant factorized at $\boldsymbol{\eta}\to0$ and we obtained expressions for the different squared eigenfrequencies:

$$\eta\to0\|z_3$$

$$\omega^2(0\,|\,\Gamma_1)=[4\lambda/3+(16/3)(k_\theta+k_{\theta'})+8\sqrt{3}K_{r\theta}+\delta+2\rho(c+d)]\frac{M_S+M_{Cd}}{M_SM_{Cd}}, \tag{3.23}$$

$$\omega^2(0\,|\,\Gamma_5)=[4\lambda/3+(16/3)(k_\theta+k_{\theta'})+8\sqrt{3}K_{r\theta}-\rho(c+d)]\frac{M_S+M_{Cd}}{M_SM_{Cd}}, \tag{3.24}$$

$$\omega^2(0\,|\,\Gamma_4{}^1)+\omega^2(0\,|\,\Gamma_4{}^2)=[4\lambda/3+(16/3)(k_\theta+k_{\theta'})+8\sqrt{3}K_{r\theta}+8\mu+2\rho(a-b)](1/M_{Cd})+[4\lambda/3+(16/3)(k_\theta+k_{\theta'})+8\sqrt{3}K_{r\theta}+8\nu+2\rho(a-b)](1/M_S), \tag{3.25}$$

$$\omega^2(0\,|\,\Gamma_4{}^1)\omega^2(0\,|\,\Gamma_4{}^2)=(1/M_SM_{Cd})[4\lambda/3+(16/3)(k_\theta+k_{\theta'})+8\sqrt{3}K_{r\theta}+8\mu+2\rho(a-b)]\times[4\lambda/3+(16/3)(k_\theta+k_{\theta'})+8\sqrt{3}K_{r\theta}+8\nu+2\rho(a-b)]-(1/M_SM_{Cd})[-2\lambda/3+(16/3)(k_\theta+k_{\theta'})+2\sqrt{3}K_{r\theta}-\delta+2\rho(c-d)]^2, \tag{3.26}$$

$$\omega^2(0\,|\,\Gamma_6{}^1)+\omega^2(0\,|\,\Gamma_6{}^2)=[4\lambda/3(16/3)(k_\theta+k_{\theta'})+2k_\theta+8\sqrt{3}K_{r\theta}+2\mu-\rho(a-b)](1/M_{Cd})+[4\lambda/3+(16/3)(k_\theta+k_{\theta'})+2k_\theta+8\sqrt{3}K_{r\theta}+2\nu-\rho(a-b)](1/M_S), \tag{3.27}$$

$$\omega^2(0\,|\,\Gamma_6{}^1)\omega^2(0\,|\,\Gamma_6{}^2)=(1/M_SM_{Cd})[4\lambda/3+(16/3)(k_\theta+k_{\theta'})+2k_\theta+8\sqrt{3}K_{r\theta}+2\mu-\rho(a-b)]\times[4\lambda/3+(16/3)(k_\theta+k_{\theta'})+8\sqrt{3}K_{r\theta}+2\nu-\rho(a-b)]-(1/M_SM_{Cd})[4\lambda/3+(4/3)(k_\theta+k_{\theta'})+5\sqrt{3}K_{r\theta}-\rho(c-d)]^2. \tag{3.28}$$

For $\boldsymbol{\eta}\|x$ we obtained two additional equations:

$$\boldsymbol{\eta}\to0\|x$$

$$\omega^2(0\,|\,\Gamma_1(T))=[4\lambda/3+(16/3)(k_\theta+k_{\theta'})+8\sqrt{3}K_{r\theta}+\delta-\rho(c'+d')]\frac{M_S+M_{Cd}}{M_SM_{Cd}}, \tag{3.29}$$

$$\omega^2(0\,|\,\Gamma_5(L))=[4\lambda/3+(16/3)(k_\theta+k_{\theta'})+8\sqrt{3}K_{r\theta}+2\rho(c''+d'')]\frac{M_S+M_{Cd}}{M_SM_{Cd}}. \tag{3.30}$$

All quantities in (3.23)–(3.30) have either been defined in (3.9), or will be given in the following few paragraphs.

Owing to the discontinuity and direction dependence of approaching a limiting value, the same modes which were Γ_1 and Γ_5 as in (3.23) and (3.24) when $\eta \to 0\|z$, become $\Gamma_1(T)$ and $\Gamma_5(L)$ as in (3.29) and (3.30) when $\eta \to 0\|x$. Thus these modes shift in frequency,[27,28] and have different polarization and selection-rule properties, as is also verified experimentally.[29]

Fit of Parameters for CdS

In Table I we give fundamental ($\eta=0$) mode frequencies and symmetries as determined by a variety of experiments in columns 1, 2, 3. The mode of frequency 256 cm^{-1} we assign as Γ_6, symmetry and that of 210 cm^{-1} we assign Γ_4. These assignments differ from those proposed by Balkanski, Besson, and Le Toullec[30]; the revised assignments were necessitated by the requirement that the eight parameters of our model be real. Our revised symmetry assignments have been subsequently (and independently) confirmed by the work summarized in columns 2 and 3 of Table I.

In column 4 of Table I we give the frequencies which we obtain as "best fit" to our model. Observe that we have achieved an exact fit of the experimental data on the assumption that recent Raman work[29] correctly gives the lowest-frequency Γ_6 mode as 44 cm^{-1}. Older work, quoted in Ref. 30, gave this as 85 cm^{-1} but the newer result seems preferable. Since the equations [(3.23)–(3.30)] are not linear, achievement of an exact fit is not a trivial result.

Using data and assignments of Table I, and (3.23)–(3.30) we find for the parameters of the model, in cgs:

$$\lambda = 1.061\times10^5 \text{ dyn/cm}, \tag{3.31}$$

$$\mu = 0.203\times10^5 \text{ dyn/cm}, \tag{3.32}$$

$$\nu = -0.086\times10^5 \text{ dyn/cm}, \tag{3.33}$$

$$\delta = -0.085\times10^5 \text{ dyn/cm}, \tag{3.34}$$

$$k_\theta = 0.170\times10^5 \text{ dyn/cm}, \tag{3.35}$$

$$k_{\theta'} = 0.154\times10^5 \text{ dyn/cm}, \tag{3.36}$$

$$K_{r\theta} = k_{r\theta} + k_{r\theta}' = -0.0216\times10^5 \text{ dyn/cm}, \tag{3.37}$$

$$\rho = 0.032\times10^5 \text{ dyn/cm}. \tag{3.38}$$

These values were used in all our calculations for wurtzite and sphalerite. For the sphalerite calculation we take $\delta=0$. Observe that the $\eta=0$ work only permits a determination of the sum of the cross-force constants $K_{r\theta}=k_{r\theta}+k_{r\theta}'$. However even for $\eta\neq0$ only the sum of these constants appears in the equations. We shall discuss the values (3.31)–(3.38) below in Sec. 5.

In addition to the springs (3.31)–(3.38), complete specification of the Coulomb field requires a statement of the values of the necessary dimensionless Ewald sums which appear in (3.23)–(3.30). These are

$$a = 5.37488, \tag{3.39}$$

$$b = 0.405219, \tag{3.40}$$

$$c = -2.12997, \tag{3.41}$$

$$d = 7.90855, \tag{3.42}$$

$$c' = 13.1457, \tag{3.43}$$

$$d' = -6.93298, \tag{3.44}$$

$$c'' = 5.50785, \tag{3.45}$$

$$d'' = 0.488606. \tag{3.46}$$

The constants (3.39)–(3.46) are the limiting, direction-dependent values of the Coulomb fields (3.19), for $\eta=0$.

TABLE I. Phonons at Γ in CdS.[a]

Symmetry	Exptl. (B)[b] (cm^{-1})	Exptl. (T)[c] (cm^{-1})	Exptl. (L)[d] (cm^{-1})	This work (cm^{-1})
Γ_1	305	305	298	298
Γ_1 (trans)	233.5	228	232	228
Γ_5 (long)		305	302	308
Γ_5	242	235	240	240
$\Gamma_6{}^1$	256	252		257
$\Gamma_6{}^2$	85	44		45
$\Gamma_4{}^1$	210			211
$\Gamma_4{}^2$	169			171

[a] One-phonon energies in CdS at Γ in the zone. Columns 2, 3, 4 from various sources, as indicated in the references, also see text. In column 5 "This work" is our fit to the values which we accept as best experimental. Observe the energy shift $\Gamma_1 \to \Gamma_5(L)$ in agreement with Ref. 3; we accept the value of 44 cm^{-1} for a Raman mode as given in Ref. 2. Our reassignment of mode symmetries is given in the Table, as explained in the text. Column 1 designations like $\Gamma_6{}^1$ and $\Gamma_6{}^2$ refer to two modes of same symmetry.
[b] Reference 30. We reassigned the 256 and 210 cm^{-1} modes, as explained in text.
[c] Reference 29.
[d] Reference 36.

4. PHONON DISPERSION AND SYMMETRY IN CdS

Wurtzite

Using the values of the spring constants (3.31)–(3.38) the secular equations (3.5)–(3.6) were solved for wave propagation in the directions Γ-A, Γ-K, Γ-M of the wurtzite zone. In each direction calculations were made at 20 equal intervals. The calculations were performed on the New York University CDC 6600 computer programmed to diagonalize complex (but Hermitian) matrices. Output was given as eigenvalues $\omega^2(\eta|j)$ and associated eigenvectors $e_\alpha(\kappa|\eta,j)$. For degenerate cases only one of the degenerate-partner eigenvectors was

[27] The frequency shifts of the Γ_1 and Γ_5 modes can also be obtained from the sum rule discussed in: M. Nusimovici and J. L. Birman, J. Phys. Chem. Solids **27**, 701 (1966).
[28] R. Loudon, *Advances in Physics* (Taylor & Frances, Ltd., London, 1964), Vol. 13, p. 423.
[29] B. Tell, T. C. Damen, and S. P. S. Porto, Phys. Rev. **144**, 771 (1966).
[30] M. Balkanski, J. M. Besson, and R. Le Toullec, in *Proceedings of the International Conference on Semiconductors, Paris, 1964* (Dunod Cie., Paris, 1965), p. 1098. See also H. Poulet and J. P. Mathieu, Compt. Rend. **258**, 2043 (1963); and K. Colbow, Phys. Rev. **141**, 742 (1966).

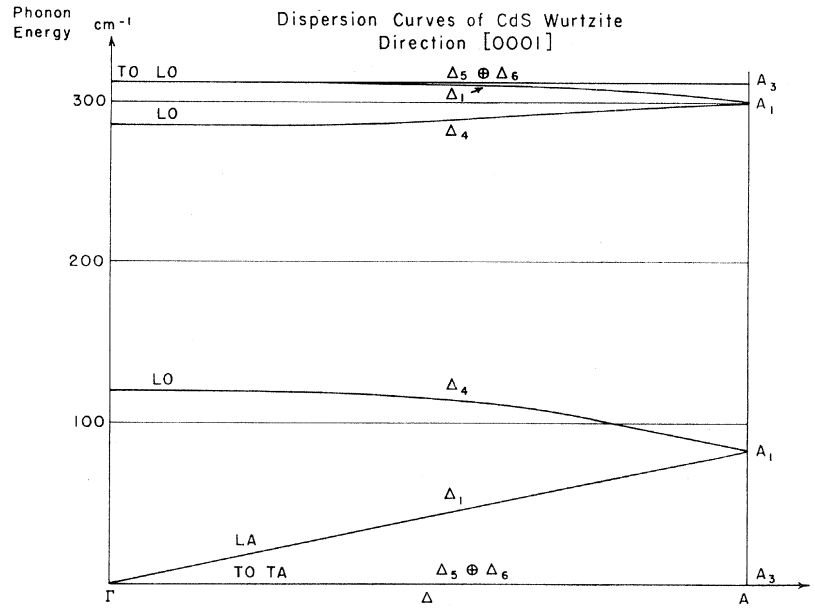

FIG. 4. Calculated phonon dispersion in CdS wurtzite, direction Γ-A. Nearest-neighbor central forces only. No Coulomb forces are included here. Observe the degeneracy of TO and LO modes, and the accidental degeneracy of Γ_5 and Γ_6. The single-force constant was adjusted so that mode frequency for TO mode was as observed (see Table I).

given by the machine. We were able to verify nonetheless in all cases that the eigenvectors transformed as partners for the irreducible representations, i.e., as members of an irreducible subspace of $\mathfrak{G}(\boldsymbol{\eta})$.[31] In cases of degeneracy, the missing partners were easily obtained using a projection operator.

Γ-A: (Wurtzite)

The symmetry of the modes for $\boldsymbol{\eta}$ at Γ was discussed above in (3.31)–(3.39); and depends as shown there on the direction of approaching Γ. For $\boldsymbol{\eta}$ at A (zone edge in the $\mathbf{b}_3$ direction) the representations spanned by the modes are

$$2A_1 \oplus 2A_3. \tag{4.1}$$

The modes A_1 are doubly degenerate and are compatible with the modes $\Delta_1 \oplus \Delta_4$ along Γ-A. Modes A_3 are fourfold degenerate, and compatible with $\Delta_5 \oplus \Delta_6$ along Γ-A.

In Fig. 4 the results of a calculation of phonon dispersion are shown for the case of a one-parameter theory, i.e., with only $\lambda \neq 0$. The value of the parameter is unimportant, since all frequencies will be proportional to $\sqrt{\lambda}$. This curve is given for comparison purposes only, and the variety of accidental degeneracies merely indicate the incompleteness of a model in which only first-neighbor short-range interactions occur. Observe in particular, that in the absence of the Coulomb field the transverse optic (TO) and longitudinal optic (LO) frequencies are degenerate at Γ. In Fig. 5 the results of our exact calculation in the direction Γ-A are shown. Among the features to be noted besides the TO-LO splitting at Γ, are the changed order of the upper A_1 and A_3 states, and the crossings of several branches in this direction.

It is also noteworthy that both our group theoretical analysis and the exact numerical calculation give no splittings of the A_3 modes. This is contrary to a surmise due to Sullivan[6]; the latter is evidently incorrect.

Γ-M: (Wurtzite)

At wave vector M the displacement representation spans the irreducible representations

$$2(2M_1 \oplus 2M_2 \oplus M_3 \oplus M_4) \tag{4.2}$$

of $\mathfrak{G}(M)$. We also can obtain the symmetrized combinations of elementary Cartesian displacements which span the irreducible subspaces (4.2), using a projection operator, and the known character tables for the irreducible representations. Let X_{I}, Y_{I}, Z_{I} be elementary unit Cartesian displacements of SI, and likewise X_{II}, Y_{II}, Z_{II} for SII, as in Fig. 1. Then if α and β are arbitrary constants (in each line) the six-dimensional representations spanned by $X_{\mathrm{I}}, \cdots, Z_{\mathrm{II}}$ may be reduced as

$$M_1: \quad \alpha(X_{\mathrm{I}}-X_{\mathrm{II}}), \beta(Z_{\mathrm{I}}+Z_{\mathrm{II}}), \tag{4.3}$$

$$M_2: \quad \alpha(X_{\mathrm{I}}+X_{\mathrm{II}}), \beta(Z_{\mathrm{I}}-Z_{\mathrm{II}}), \tag{4.4}$$

$$M_3: \quad \alpha(Y_{\mathrm{I}}+Y_{\mathrm{II}}), \tag{4.5}$$

$$M_4: \quad \alpha(Y_{\mathrm{I}}-Y_{\mathrm{II}}). \tag{4.6}$$

Particularly noteworthy is the occurrence of z bases among the nontrivial representations M_2. This result differs from assertions previously made, by workers in the field.[4,14,15] We checked the basis (4.3)–(4.6) upon the computed eigenvectors. Of course, in addition to the S

[31] G. Y. Lyubarski, *The Application of Group Theory in Physics* (Pergamon Press, Inc., New York, 1960); J. L. Birman, in *Handbuch der Physik*, edited by S. Flügge (Springer-Verlag, Berlin, to be published), Vol. XXV/2.

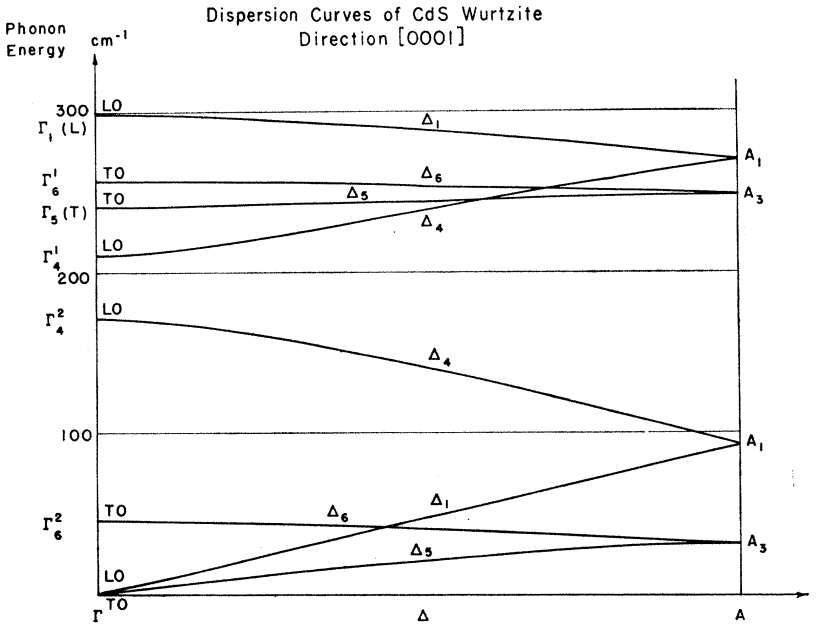

FIG. 5. Calculated phonon dispersion CdS wurtzite, direction Γ-A. Results presented including valence and Coulomb force field contributions. Compare with Fig. 4 for Coulomb splittings, lifting of some, and production of other, accidental degeneracy.

displacements, Cd displacements must be considered; but these essentially duplicate the results (4.3)–(4.6).

In Fig. 6 our calculated eigenfrequencies in direction Γ-M are shown.

Γ-K: (Wurtzite)

At wave vector K the displacement representation spans

$$2(K_1 \oplus K_2 \oplus 2K_3), \tag{4.7}$$

of $\mathfrak{G}(K)$. Using the same Cartesian displacement trial space here for K as above for M we find as subspaces:

$$K_1\text{: } (X_\mathrm{I}-X_\mathrm{II})+i(Y_\mathrm{I}+Y_\mathrm{II}), \tag{4.8}$$

$$K_2\text{: } (X_\mathrm{I}+X_\mathrm{II})+i(Y_\mathrm{I}-Y_\mathrm{II}), \tag{4.9}$$

$$K_3\text{: } \begin{Bmatrix} \alpha[(X_\mathrm{I}+X_\mathrm{II})-i(Y_\mathrm{I}-Y_\mathrm{II})], \beta Z_\mathrm{I} \\ \alpha[(X_\mathrm{I}-Y_\mathrm{II})-i(Y_\mathrm{I}-Y_\mathrm{II})], \beta Z_\mathrm{II} \end{Bmatrix}. \tag{4.10}$$

Again observe that the z displacements are to be found in the K_3 subspace in contradiction to earlier work.[4,14,15]

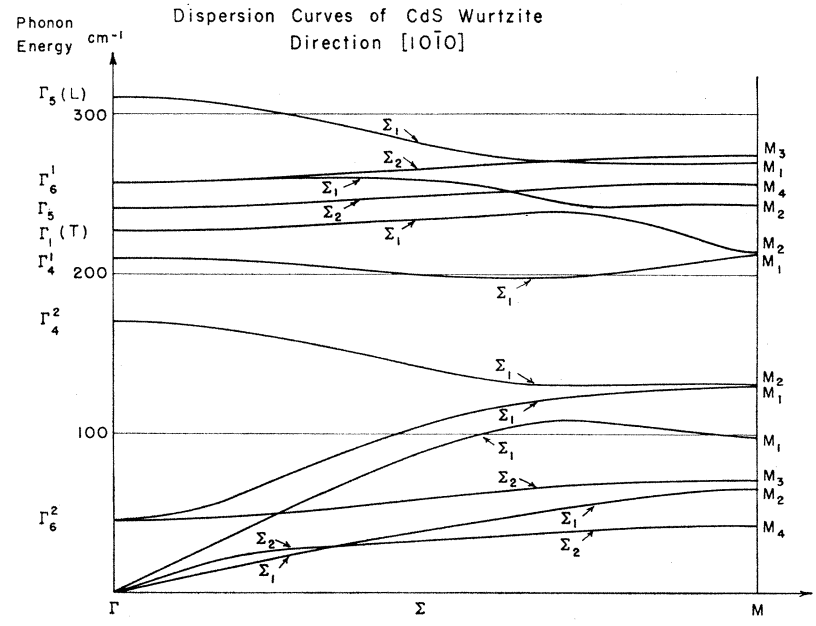

FIG. 6. Calculated phonon dispersion CdS wurtzite, direction Γ-M. Results include valence and Coulomb force field contributions.

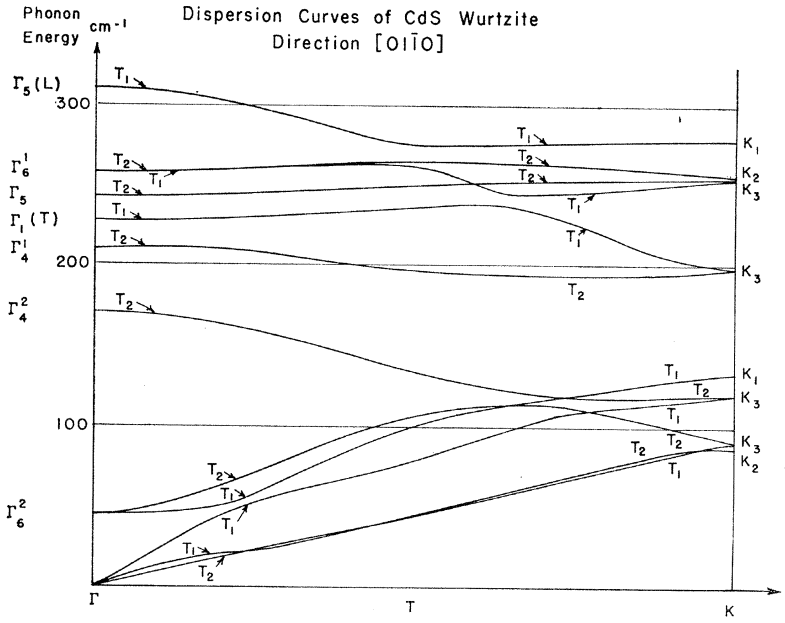

FIG. 7. Calculated phonon dispersion CdS wurtzite, direction Γ-K. Results include valence and Coulomb force field contributions.

Calculated eigenvectors verify these assignments of bases, again adding the Cd degrees of freedom.

The calculated phonon dispersion results in direction Γ-K are given in Fig. 7.

Critical-Point Phonons (Wurtzite)

Rashba[15] has given an analysis of the vanishing of the matrix elements of the operator ∇_η, which is relevant to the enumeration of the analytic critical points[32] in wurtzite. At such a point, one or more components of $\nabla_\eta\omega(\eta|j)=0$, for the branch j. From Figs. 5, 6, and 7 it is very likely that there are other critical points due to dynamic effects, i.e., "accidental degeneracies" (or crossings of the dispersion surfaces, not due to symmetry) as well as vanishing slopes, components of $\nabla_\eta\omega(\eta|j)$, along symmetry lines. Comparing Figs. 4 and 5 we can observe how the change in the dynamics by inclusion of the Coulomb-field effects, causes additional crossings of the Δ_4, Δ_5, and Δ_6 curves.

In the present paper we did not carry out a detailed density-of-states analysis of phonon dispersion throughout the entire zone, consequently we do not present a list of the calculated critical points.[33] Rather, in Table II we give a listing of our calculated values of phonon frequencies at those wurtzite critical points for which the calculation was carried out: Γ, A, K, M. The values given will be used below in our interpretation of the observed[29] 2-phonon Raman scattering spectrum in CdS.

One-phonon and two-phonon density of states have been calculated from our model and will be reported elsewhere.

TABLE II. Phonons at critical points in CdS wurtzite.

Point Γ (cm^{-1})	Point A (cm^{-1})	Point K (cm^{-1})	Point M (cm^{-1})
$\eta\to 0\|\|z$ axis			
Γ_1 0	A_3 32	K_2 89	M_4 43
Γ_5 0	A_1 93	K_3 90	M_2 68
Γ_6 45	A_3 249	K_3 120	M_3 71
Γ_4 171	A_1 270	K_1 133	M_1 99
Γ_4 211		K_3 198	M_1 130
Γ_6 257		K_3 254	M_2 131
Γ_5 240		K_2 257	M_1 214
Γ_1 298		K_1 279	M_2 215
$\eta\to 0\perp z$ axis			M_2 243
$\Gamma_1(T)$ 228			M_4 257
$\Gamma_5(L)$ 308			M_1 269
			M_3 275

Sphalerite

For sphalerite we used the values of the spring constants (3.31)–(3.38) except for the two modifications, previously mentioned. The third-neighbor constants δ was taken to vanish: $\delta=0$. For the Coulomb part of the dynamical matrix, the dipole sums **B** were all recalculated in the two directions in which the phonon dispersion was calculated, using the correct geometry for sphalerite and the exact Ewald method. In this manner the 6×6 dynamical matrix was constructed, and the secular equations (3.5)–(3.6) solved for waves propagating in the direction Γ-Λ (or Γ-L), and Γ-M sphalerite structure of CdS.

Γ-Λ: (Sphalerite)

In sphalerite the mode symmetries at $\eta=\Gamma=0$ are classified according to irreducible representations of

[32] L. van Hove, Phys. Rev. 89, 1189 (1953); J. C. Phillips, *ibid.* 104, 1263 (1956).

[33] As given, for example, by F. A. Johnson and R. Loudon, Proc. Roy. Soc. (London) A231, 274 (1964) for diamond, germanium, and silicon.

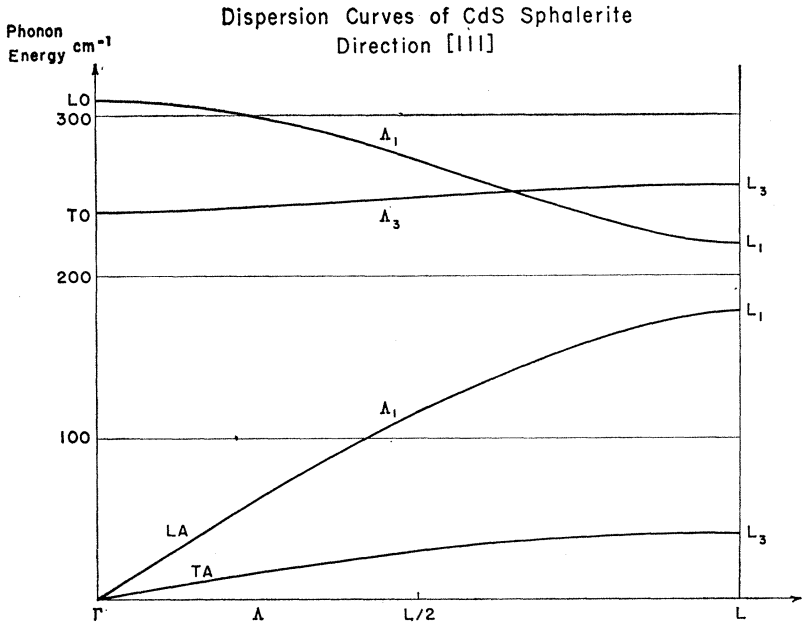

FIG. 8. Calculated phonon dispersion in CdS sphalerite, direction Γ-L. Results include valence and Coulomb force field contributions.

$\mathfrak{G}(\Gamma)/\mathfrak{T}=T_d$. Omitting the Coulomb field, the displacement representation spans[4]

$$2\Gamma_{15}, \tag{4.11}$$

of which one Γ_{15} corresponds to the acoustic modes with $\omega^2(0|\Gamma_{15})=0$. The other optic triple is split by the Coulomb field into a doubly degenerate TO and a higher LO. At L, which has no higher symmetry than points on Λ, the line joining Γ-L, the modes span representations

$$2L_1\oplus 2L_3 \tag{4.12}$$

of the little group.

In Fig. 8. the calculated phonon spectrum of a sphalerite CdS is shown in this direction. Note the mark on the abscissa in the figure corresponding to a wave vector whose magnitude is half the maximum ($\eta=L/2$). This "corresponds" to the wave vector A of wurtzite.[4]

Γ-M: (Sphalerite)

The direction Γ-M in sphalerite is one of low symmetry with the modes being classified along the direction, as well as at the end point M, only as even or odd under the mirror plane which is the only operation in

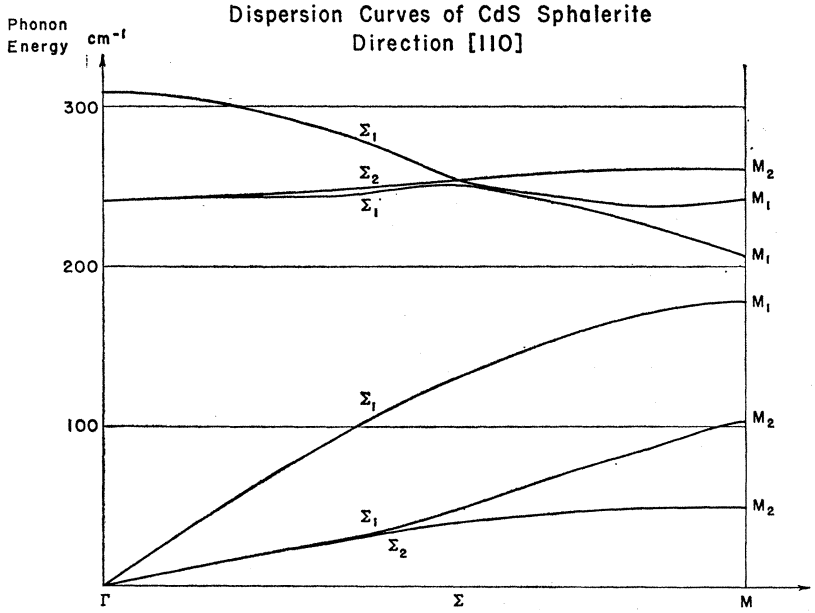

FIG. 9. Calculated phonon dispersion in CdS sphalerite, direction Γ-M. Results include valence and Coulomb force field contributions.

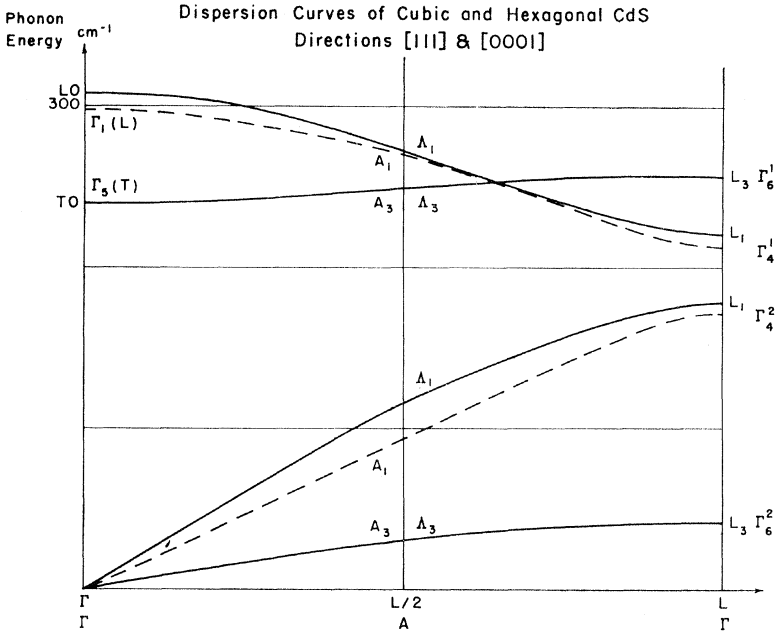

FIG. 10. Comparison of phonon dispersion in CdS wurtzite and CdS sphalerite. The wurtzite Γ-A-Γ curve (Fig. 5) has been "unfolded" to correspond to sphalerite Γ-L (Fig. 8) and both then plotted on a common scale. In the figure, the transverse modes (acoustic curve labeled Γ-A-Γ_3 and optic curve labeled TO-A_3-L_3) are identical in corresponding wurtzite and sphalerite. The longitudinal modes differ (solid curve is sphalerite, dashed curve is wurtzite). The sphalerite longitudinal branch is at higher frequency than the corresponding wurtzite branch.

$\mathfrak{G}(M)/\mathfrak{T}$. The representations spanned are

$$2M_1 \oplus 4M_2. \tag{4.13}$$

In Fig. 9 the calculated phonon spectrum of sphalerite CdS is shown in the direction Γ-M. On comparing Fig. 9 with Fig. 8 one observes certain similarities in energies of the highest optical, and the acoustic, branches in the two cases, at the zone end points M. As discussed elsewhere[4] the matter of comparison of wave propagation (electron or phonon) sphalerite and wurtzite in these two directions is neither simple nor unambigous. In Table III computed phonon energies at Γ, L, and M are given for CdS sphalerite.

Comparison of CdS Wurtzite and Sphalerite

The directions Γ-A-Γ in wurtzite and Γ-L in sphalerite may be compared since planes of constant phase are similar in the two cases.[4,12] To facilitate the sphalerite-wurtzite comparison we plot the phonon dispersion curves along Γ-L in sphalerite and along Γ-A-Γ in wurtzite, on a common $\omega(\eta)$ plot in Fig. 10. To obtain the wurtzite result we "unfolded" the wurtzite Brillouin zone[4] as shown in Fig. 3. Results immediately apparent from observation of Fig. 10, and Tables II and III are that:

(a) The sphalerite transverse frequencies are identical with their wurtzite counterparts.

(b) The sphalerite longitudinal frequencies are at larger energy than their wurtzite counterparts.

TABLE III. Phonons in CdS sphalerite.

Point Γ (cm^{-1})	Point M (cm^{-1})	Point L (cm^{-1})
LA 0	M_2 51	L_3 42
TA 0	M_1 109	L_1 178
TO 240	M_1 180	L_1 220
TO 308	M_1 207	L_3 257
	M_1 242	
	M_2 261	

5. DISCUSSION AND CONCLUSION

The most valid comparison of our results with experiment would rely upon a comparison of calculated phonon frequencies with those measured, for example by inelastic neutron scattering. To our knowledge, the only wurtzite material for which phonon frequencies have been so found[9] is BeO.

Consequently we must examine other more indirect possible checks of our calculation. One possibility is multiphonon optical spectra, due to infrared[30] or Raman[29] processes. In view of the "weakness" of the selection rules[16] for infrared multiphonon processes, which allow almost all combinations we examined the observed two-phonon Raman spectrum.[29] We shall give our interpretation of the seven observed active two-phonon processes, using the selection rules, plus our numerical calculation for wurtzite. As is usual in work of this kind,[34,35] we restrict attention to the allowed multiphonon processes originating from those critical point phonons whose energy we calculated. In essence this approximation replaces the actual crystal and its oscillators by a collection of discrete Einstein

[34] J. L. Birman, Phys. Rev. **131**, 1489 (1963).

[35] F. A. Johnson and R. Loudon, Proc. Roy. Soc. (London) **A281**, 274 (1964); H. Bilz, R. Geick, and K. Renk, in *Lattice Dynamics*, edited by R. F. Wallis (Pergamon Press, Inc., New York, 1965), p. 355.

oscillators of frequency and symmetry corresponding to the critical points used. Even so, it should be noted that we did not calculate phonon frequencies for all the critical points.[15] In Table IV this interpretation is given. It can be seen that we are able to account in a simple way for all observed two-phonon energies in terms of various combinations and overtones, consistent with selection rules. A complete comparison of infrared and Raman multiphonon observations and our theory in CdS, involves calculation of the joint multiphonon density of states. This comparison will be reported later.

An important check on our calculation was already mentioned earlier in discussing the fit of the one-phonon optical data. In order to fit our springs to real values, we found it necessary to alter the symmetry assignment of two of the phonons: the 210-cm^{-1} mode symmetry Γ_4, and the 256-cm^{-1} mode of symmetry Γ_6. The revised interpretation given in Table I was confirmed independently, and subsequent to our work by Raman scattering.[29] Since all springs appear in the equations for these mode eigenfrequencies, this tends to confirm the validity of the model used.

Additional one-phonon confirmation of our model can be observed from Table I. We predict displacement of both the Γ_1 and Γ_5 modes when observed for $\boldsymbol{\eta}\|x$ compared to $\boldsymbol{\eta}\|z$. In very recent work, Le Toullec has observed the predicted shift in the infrared absorption.[36] This predicted displacement was not observed in Raman scattering.[29] We cannot explain the lack of observation of the shift by Raman scattering, unless this is a "dynamical" effect involving a numerically low cross section. Also, regarding one-phonon energies, infrared absorption of CdS sphalerite and wurtzite suspensions (pressed powders) and films have been reported.[37] The sphalerite structure was reported to show a higher-frequency "strong absorption band" than wurtzite. No quantitative data was given, so the significance of the report is difficult to determine. However, the reported shift of peak frequency of 10 cm^{-1} from 260 cm^{-1} (wurtzite) to 270 cm^{-1} (sphalerite) corresponds to our calculated difference in LO frequencies, see Fig. 10, and Table I and Table III. Since the electrostatic field in a small particle (or film) is shape-dependent, and hence also the LO-TO frequency shift, this numerical agreement should be considered as possibly fortuitous.

A reasonable feature of our model is the numerical values of the short-range force constants (3.31)–(3.38) If we compare our force constants to those obtained by Musgrave and Pople in their treatment of diamond, then we easily see that our short-range force constant λ scales in accord with a simple rule: $\omega^2=\lambda/m$, where ω is a typical Raman frequency, m the appropriate (reduced) mass. The reduced mass appropriate for wurtzite is $(M_S M_{Cd})^{1/2}=60$; that for diamond $M_C=12$; Raman frequencies 298 cm^{-1}, versus 1332 cm^{-1}, respectively. Taking the diamond first-neighbor spring constant[21] as about 4.5×10^5 dyn/cm, a "scaled" CdS spring constant would be about 1.1×10^5 dyn/cm. This agrees with our result (3.31), which includes only bond stiffness. The angle stiffnesses k_θ and $k_{\theta'}$ also scale properly at about 0.1λ as in valence force models of this kind[24] and in agreement with the work of Musgrave and Pople.[38] The Coulomb parameter ρ may be used to compute an effective charge. We find in this way ion charges $|q|\sim1.0|e|$; this is in reasonable agreement with the Szigetti charge[39] of $0.7|e|$. Thus the model parameters of the valence force field part of our model have values in good agreement with other work of this kind, and likewise the Coulomb-field parameter appears correct.

Using our calculated dispersion curves, the velocity of sound for elastic wave propagation parallel and perpendicular to z was computed. Results are presented

TABLE IV. Two-phonon Raman scattering in CdS wurtzite.[a]

Experiment[b] (cm^{-1})	Interpretation	Calculation (cm^{-1})
97	$2\Gamma_6$	90
	$2M_4$	86
207	$M_1\oplus M_3$	201
	$M_2\oplus M_3$	202
	$K_2\oplus K_3$	209
	$K_3\oplus K_3$	210
328	$M_2\oplus M_4$	323
	$M_3\oplus M_4$	328
	$K_1\oplus K_3$	331
347	$A_1\oplus A_3$	342
	$M_1\oplus M_2$	345
	$M_1\oplus M_1$	344
	$M_2\oplus M_2$	346
	$M_1\oplus M_2$	342
	$M_3\oplus M_3$	346
	$K_2\oplus K_3$	347
	$K_2\oplus K_2$	346
	$K_3\oplus K_3$	344
	$K_3\oplus K_2$	346
364	$A_1\oplus A_1$	363
	$K_1\oplus K_2$	368
	$K_1\oplus K_3$	369
	$M_1\oplus M_1$	368
556	$2K_1$	558
	$2M_3$	550
605	$2\Gamma_1$	596
	$2\Gamma_5(L)$	616

[a] Interpretation of the observed two-phonon Raman scattering processes in CdS wurtzite in terms of permitted two-phonon processes with energies as calculated by the valence-Coulomb field as described in the text.
[b] Reference 29.

[36] R. Le Toullec (private communication).
[37] A. Mitsuiski, H. Yoshinaga, and S. Fujita, J. Phys. Soc. Japan **13**, 1235 (1958).
[38] M. J. P. Musgrave (private communication).
[39] Reference 17, Chap. II. Also P. Aigrain and M. Balkanski, *Selected Constants Relative to Semiconductors* (Pergamon Press, Inc., New York, 1961).

TABLE V. Velocity of sound in CdS.[a]

Propagation direction	Calculated (m/sec)		Experiment[b] (m/sec)
$\parallel z$	LA	4000	4500 (C_{33})
	TA	1850	1850 (C_{44})
$\perp z$	LA	4300	4300 (C_{11})
	TA($\perp z$)	2500	3350 (C_{66})
	TA($\parallel z$)	1800	1806 (C_{44})

[a] Calculated elastic constants using calculated phonon dispersion in Figs. 5–7.
[b] Measured elastic constants taken from D. Berlincourt, H. Jaffe, and L. R. Shiozawa [Phys. Rev. 129, 1009 (1963)]. Parentheses indicate elastic constants involved in the indicated phase velocity.

in Table V, and compared with experiment. In most cases a respectable agreement has been achieved. The only serious discrepancy is for the phase velocity involving the elastic constant c_{66}, corresponding to a transverse-polarized mode propagating perpendicular to the $\mathbf{a}_3$ or z axis.

In all ways immediately accessible to us, the predictions of our calculation appear in satisfactory accord with experiment. Comparing the one-parameter (first-neighbor bonds only) model results given in Fig. 4, with the results in Fig. 5 we see clearly the qualitative and quantitative importance of both valence (short-range) and Coulomb (long-range) contributions to the force field in CdS. Since work on mixed crystals of various stoichiometries in the wurtzite and zincblende structures is now under way,[40] it seems likely that, as a matter of principle the quantitative interpretation of these results too, for compounds like CdS:CdSe will necessitate the proper inclusion of both short-range valence and long-range Coulomb forces. The relative significance of short-range versus long-range forces can be quantitatively appreciated from the magnitude of the contribution of the particular "spring" to the particular frequency in which it appears. Observe that the Coulomb spring ρ appears at $\eta=0$ with the dimensionless lattice sums, $a, b, c, d, c', d', c'', d''$, whose values are tabulated in (3.39)–(3.46). Clearly in a partially ionic material like CdS (or Cd:Se, etc.) the Coulomb field not only provides qualitative splittings such as Γ_1-Γ_5 but also quantitatively locates the frequencies as is seen from inspection of the equations (3.21)–(3.30).

It is apparent that a central problem in lattice-dynamic studies is the correct inclusion of a proper mixture of long- and short-range forces.[41,42] It was the failure of oversimplified short-range (valence) force models to account for experiments which led to introduction of a pseduo-long-range interaction via shell-model displacements in dealing with germanium and silicon; conversely, the rigid-ion purely long-range forces required modification via introduction of short-range deformation dipoles in addition to the usual overlap repulsion in the alkali halides. Even these models are not entirely satisfactory, and basic modifications are still being made in these models, e.g., via the introduction of additional parameters,[7] some of which have no evident physical meaning, or new models such as the "breathing-shell model."[43] The situation is then such that no single model is completely satisfactory for all materials. The present work, in the context of related studies[18,19,21,22] indicates one way in which a model may be designed to include both the short-range and long-range fields, via a combination of valence forces and Coulomb forces, which may have general validity for materials with mixed binding.

ACKNOWLEDGMENTS

We wish to thank Dr. M. J. P. Musgrave with whom we have discussed various aspects of valence force field calculations, including the present work. Conversations with Professor Harvey Kaplan, Professor H. Bilz, and Dr. R. Cowley were also helpful in various ways. Dr. R. Le Toullec kindly communicated his recent infrared measurements in CdS to us in advance of publication. Finally it is a pleasure to thank Professor M. Balkanski for his interest.

[40] M. Balkanski, R. Besserman, and J. M. Besson, Solid State Commun. 4, 201 (1966); H. Verleur and A. Barker, Phys. Rev. 149, 715 (1966); Y. S. Chen, W. Shockley, and G. L. Pearson, *ibid.* 151, 648 (1966); D. W. Langer, Y. S. Park, and R. N. Euwema, *ibid.* 152, 788 (1966).

[41] M. Lax, in *Lattice Dynamics*, edited by R. Wallis (Pergamon Press, Inc., New York, 1965), p. 179.

[42] A. M. Karo and J. R. Hardy, Phys. Rev. 141, 696 (1966), and references therein.

[43] U. Schroeder (private communication, courtesy of Professor H. Bilz).